

A SEDIMENTARY RECORD OF THE ENVIRONMENTAL EVOLUTION AND CHANGES IN TROPHIC STATE OF SAN ROQUE RESERVOIR (CÓRDOBA, ARGENTINA) DURING THE 20TH- 21ST CENTURIES

Luciana Mengo ^{1*}, Silvana Halac ¹, Gabriela Foray ², Ingrid Costamagna ¹, Eduardo Piovano ¹

¹ Centro de Investigaciones en Ciencias de la Tierra (CICTERRA), Consejo Nacional de Investigaciones Científicas y Técnicas CONICET). Universidad Nacional de Córdoba. Av. Vélez Sarsfield 1699, X5016, Córdoba, Argentina.

² Centro de Excelencia en Productos y Procesos de Córdoba (CEPROCOR). Ministerio de Ciencia y Tecnología. Gobierno de la Provincia de Córdoba. Pabellón CEPROCOR, X5164, Santa María de Punilla, Córdoba, Argentina.

* Corresponding author: luci.92.22@gmail.com

ARTICLE INFO

Article history

Received July 6, 2021

Accepted September 24, 2021

Available online September 28, 2021

Handling Editor

Sebastian Richiano

Keywords

Paleolimnology

Fossil pigments

Hydroclimatic variability

Land-use change

Water quality

Semiarid region of central Argentina

ABSTRACT

Paleolimnological studies have been widely used to establish the past conditions of lakes and reservoirs due to both anthropic impact and climatic influences. The San Roque reservoir (SRr) is located in a semiarid region of central Argentina and has reached a hypereutrophic state in the last two decades. The main aim of this study is to reconstruct the environmental history of the SRr. The sedimentological record of the SRr, along with its chronology, provides a detailed archive of environmental changes. The multi-proxy analysis of the paleolimnological record makes it possible to identify four main environmental stages throughout the history of the SRr, resulting from the action of natural and anthropic drivers. Stage 1 (1911–1958 CE) can be considered the environmental base level of the reservoir as anthropic activity then was the lowest of all the stages. Stage 2 (1958–1978 CE) represents an increase in the volume of the SRr as a result of the construction of a second dam, along with a generalized increase in regional precipitation at the end of the period. Stage 3 (1978–2000 CE) is characterized by an increase in the internal primary production (eutrophic state), mainly caused by an anthropic input of nutrients (e.g., sewage effluents) due to urban expansion in the fluvial catchment. Stage 4 (2000–2018 CE) corresponds to the highest trophic scenario in the SRr, which has led to a hypereutrophic state. This is mainly associated with the increase in urbanization throughout the catchment and, especially, in the littoral area of the reservoir. The environmental reconstruction indicates that the SRr has been impacted by different types of disturbances throughout its history, including an enlargement of its volume due to the construction of the second dam and the higher nutrient load resulting from the increased urbanization. In addition, the great hydroclimatic jump after the 70s may have influenced these processes. Our results mostly highlight that anthropic and natural forcing synergistically promoted the generalized degradation of SRr water quality. These results can provide tools for modeling future scenarios and improving watershed management policies.

INTRODUCTION

Paleolimnology has been used for decades to reconstruct past climatic variability and, more recently, to identify environmental changes due to anthropic impact (Saulnier-Talbot, 2016; Dubois *et al.*, 2018). Paleolimnological data provide invaluable tools to elucidate temporal shifts in the biophysicochemical dynamics within lakes and their catchments (Cohen, 2003; Paterson *et al.*, 2020). Lake archives provide continuous records of long-term environmental change gathering information from their airsheds and watersheds. Therefore, in order to reconstruct past environmental conditions, it is necessary to look into the past by using environmental proxies such as physical (*e.g.*, sedimentary facies, sediment magnetic properties, structures, grain-size), geochemical (*e.g.*, organic matter content, chemical elements, biomarkers), or biological (*e.g.*, diatoms, chironomids, cladocerans, chrysophytes) indicators (Birks and Birks, 2006; Pienitz and Lotter, 2009).

Recent studies have shown that reservoir sedimentary records provide high resolution archives of past environmental variability (Winston *et al.*, 2014; Wengrat *et al.*, 2018, 2019; Gangi *et al.*, 2020; Halac *et al.*, 2020). Thus, paleolimnology has become a successful tool to further decipher the response of artificial water bodies faced with environmental stressors such as human activity and hydroclimatological changes (Costa-Böddeker *et al.*, 2012; Moorhouse *et al.*, 2018; Wang *et al.*, 2021). In addition, paleolimnology becomes an effective tool to establish the environmental base condition of natural and artificial lakes, something which is usually difficult to establish due to a lack of information spanning pre-monitoring periods, which do not normally go back longer than 30 years (Pienitz and Vincent, 2003; Woodbridge *et al.*, 2014). Knowledge of the initial condition is essential to establish water quality assessment and proper management of catchments (Smol, 2010).

It is known that the water quality of reservoirs around the world has deteriorated as a result of changes in trophic status, many of which have reached hypereutrophic levels (Padedda *et al.*, 2017; Oliver *et al.*, 2019). Recently, paleolimnology has focused on the evolution of aquatic systems deterioration linked to multiple causes such as human activity and climate change (Dearing, 2013;

Saulnier-Talbot, 2016; Moorhouse *et al.*, 2018; Wang *et al.*, 2021). The acceleration of eutrophication during recent decades has seriously deteriorated the water quality of a large number of reservoirs in South America, most of which were built as drinking water supplies for many urban locations (Roldán Pérez and Ramírez Restrepo, 2008; Cardoso-Silva *et al.*, 2018; Gangi *et al.*, 2020).

Drivers triggering environmental changes in reservoirs may include those in the hydrological balance (*i.e.*, rainfall variability and river discharges, Elchyshyn *et al.*, 2018; Kennedy, 2005), land-use change (*e.g.*, urban growth and emission of effluents, Moorhouse *et al.*, 2018; Schroeder *et al.*, 2016; Winston *et al.*, 2014), deforestation and soil erosion (Ye *et al.*, 2014; Krasa *et al.*, 2019), fires (Bonansea and Fernandez, 2013), as well as lake management policies such as level control (Xu *et al.*, 2019).

Although reservoirs are vitally important water supplies in the semiarid central region of Argentina (Dasso *et al.*, 2014), the noticeable lack of long-term monitoring and paleolimnological studies hamper the long-term evaluation of water quality changes. Our research aims to reconstruct the environmental evolution of a reservoir located in the central semiarid region of Argentina, and to identify the most important natural and anthropic drivers. The site of study, San Roque reservoir (SRr), is the main source of drinking water for the city of Córdoba (1.3 million inhabitants). The goals of this work are: i) to reconstruct the environmental history of the SRr for the last 100 years through a paleolimnological analysis; ii) to determine the influence of both regional natural and anthropic drivers on the evolution of the environmental state of the SRr; iii) to establish the environmental base condition of the SRr, when the anthropic impact in the catchment was low or negligible. These results provide valuable information for the development of management policies for the reservoir and its fluvial catchment under future scenarios of climate change and growing anthropic pressures.

General setting

The SRr (31° 22' S, 64° 27' W; Fig. 1a) is located in the semiarid region of central Argentina at 608 m asl (meters above sea-level) in the Punilla Valley between the Sierras Chicas and Sierras Grandes in Córdoba, Argentina (Martino *et al.*, 2012). SRr is a

multipurpose reservoir which supplies drinking water to more than one million inhabitants in the city of Córdoba and surrounding areas, as well as providing flood control, power generation, recreation and tourism. It was developed in two stages. The first dam, built between 1881 and 1891, was replaced in 1944 by the current dam, enlarging the capacity of the reservoir from 112 to 201 hm³ (Ballester, 1931). Changes in reservoir morphometry occurred after the second dam construction can be seen in geological maps corresponding to different years (1932 CE: <https://repositorio.segemar.gov.ar/handle/308849217/570>; 2000 CE: <https://repositorio.segemar.gov.ar/handle/308849217/2097>). The surface area and volume of the reservoir are 15 km² and 201 hm³ respectively, the average water depth is 13 m, and maximum water depth is 35 m, close to dam (see bathymetry in Fig. 1).

The SRr catchment has a surface area of 1750 km² (Merlo *et al.*, 2011; Monferrán *et al.*, 2011) and is composed of igneous and metamorphic rocks (Martino *et al.*, 2012). The SRr is fed by four main tributaries (Fig. 1a), the San Antonio and Cosquín rivers and Los Chorrillos and Las Mojarras streams, while the Suquía River is the only effluent (Rodríguez and Ruiz, 2016). The regional climate is semihumid to semiarid. Mean annual precipitation is 780 mm, while total annual precipitation may range between 400 and 1000 during dry or wet years respectively (Pasquini *et al.*, 2006; Colladón, 2014). The annual rainfall pattern is seasonal, with a wet season from October to April (Colladón, 2014). The climate has a high diurnal temperature variation with a mean annual temperature of 14°C and minimum and maximum mean values of 7°C and 24°C, respectively (Colladón, 2004). The SRr catchment is located in the Chaco Serrano district, which has native forest between 500 and 1300 m asl. There is a major proportion of grasslands above 1000 m asl, where bare soil is developed (Cabrera, 1971; Cabido and Zak, 1999).

The land-use in the SRr catchment is restricted mainly to grassland management associated with cattle and poultry breeding, while a small portion of the watershed is occupied by forest plantations (Fig. 1a). During recent decades, the population and urban development in the Sierras Chicas region have increased markedly (Deon, 2015). The change of land-use to urban occupation has increased noticeably in the cities of Villa Carlos Paz, Cosquín

and La Falda, and in several small villages located next to San Antonio River and Los Chorrillos stream, e.g. Cuesta Blanca and Tanti, respectively (Fig. 1b).

During the last three decades, the rate of urbanization has increased by more than 200%, rising from 19 km² to 46 km² throughout the basin (Fig. 1b). However, during the same period, the urbanization fringing the SRr littoral area, e.g., the city of Villa Carlos Paz, the main urban center of the SRr basin, has grown more than 300%. The growth of urbanization at the southern area occurred in the late 90s (San Antonio River area) while during the 21st century the urban expansion took place in the southwestern area (Fig. 1c).

Preliminary results indicate that the water quality of the reservoir has shown conspicuous deterioration since the mid-1970s (Bonetto *et al.*, 1976). Nowadays, the water quality is still decreasing drastically due to the large unplanned urban development in the SRr basin, which results in the delivery of untreated sewage discharges from direct and diffuse sources. Other anthropic activities like deforestation and fires also contribute to the increase of allochthonous organic matter and sediment delivery to the SRr (Rodríguez and Ruiz, 2016). In this context, several processes intensified at the SRr during the last decade, including changes on its trophic state (from eutrophic to hypereutrophic), occurrence of recurrent cyanobacteria blooms, the development of hypolimnetic anoxia conditions and fish death, among others (Rodríguez and Ruiz, 2016; Halac *et al.*, 2020).

MATERIALS AND METHODS

Core sampling, sedimentary description and geochemistry

A 94-cm-long sedimentary core (TSR-18-I) was collected in December 2018, using a gravity corer (IQTEC, “Bob corer type”). The core was retrieved in the central area of the reservoir (31° 22' 42" S; 64° 28' 19.4" W; Fig. 1d) at a water depth of 18 m. The coring site is located at 4.5 km of Cosquín-Las Mojarras fluvial mouths, at 3.1 km of San Antonio-Los Chorrillos fluvial mouths, and at 0.7 km of the west lake shoreline. The core was stored at 4°C within 1-2 h after collection at the GeoLimnoLab, CICTERRA, Córdoba, Argentina.

Computed tomography images were obtained to

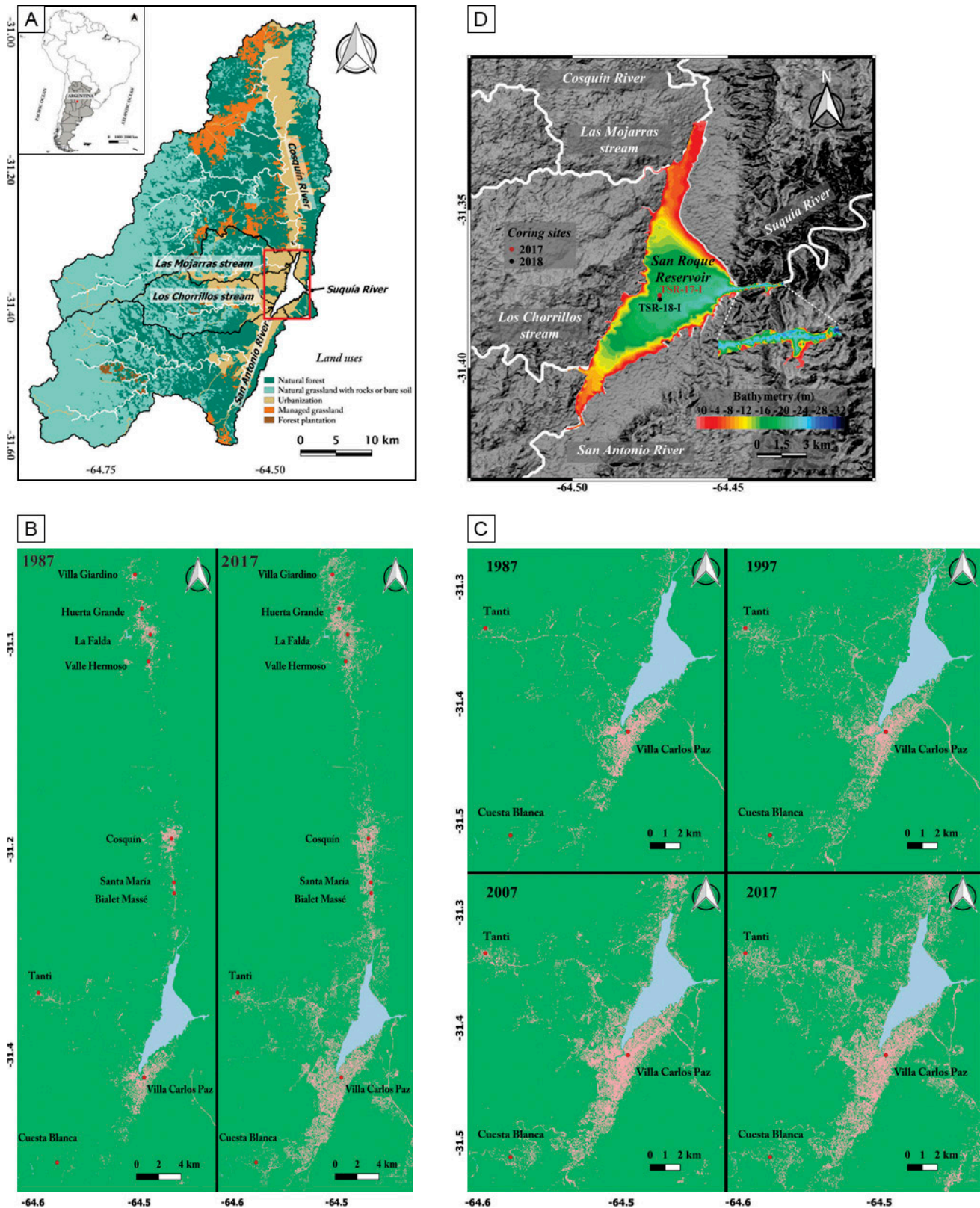


Figure 1. a) Location of San Roque reservoir in South America and in Central Argentina. San Roque catchment land uses, main tributaries (San Antonio and Cosquín Rivers, and Las Mojarras and Los Chorrillos streams) and the effluent (Suquía River) are indicated. b) and c) Spatiotemporal urban growth in the San Roque reservoir catchment area and in the littoral area of San Roque reservoir, respectively. Urban growth was estimated by multi-temporal analysis of Landsat 5 (1987, 1997, and 2007) and Landsat 8 (2017) satellite images. d) Bathymetry of San Roque reservoir (2016 CE; Gomez et al., 2016). Location of coring site TSR-18-I and TSR-17-I in San Roque reservoir. Main tributaries and the effluent are indicated.

recognize fine-scaled sedimentary structures in the undisturbed sedimentary core. Then the core was cut in two halves and photographed. An initial core description was made following the criteria proposed by the Limnological Research Center Core (<http://lrc.geo.umn.edu/laccore/icd.html>) and according to Schnurrenberger *et al.* (2003). The magnetic susceptibility (MS) of the sediments was measured on the surface of the split half core at 1 cm intervals with a MS2E Bartington sensor at the GeoLimnoLab. Values were expressed in 10^{-5} SI (dimensionless). Sediment samples were taken continuously every 1 cm, or at each macroscopic sedimentological change.

Sediment water content (H_2O) was determined by weighing the subsamples before and after drying at $105^\circ C$ for 24 h. Total Organic and Inorganic Carbon content (TOC and TIC) were determined by loss-on-ignition (LOI) and obtained by weighing the samples after heating at $550^\circ C$ and $950^\circ C$, respectively (Dean, 1974; Heiri *et al.*, 2001). The amount of organic carbon was estimated from the mass loss (percentage of dry weight) after combustion at $550^\circ C$ (LOI $550^\circ C$), multiplied by 0.5. Subsequent mass lost after combustion at $950^\circ C$ multiplied by 1.36 (the ratio between the molecular weights of CO_3 and CO_2) gives a theoretical mass of carbonate in the sample.

Relative density values of sediments were estimated from the computer tomography images using the free software ImageJ (Foucher *et al.*, 2020). The obtained values were further calibrated using the dry bulk density ($g \cdot cm^{-3}$), which was also calculated according to Binford *et al.* (1993) at a centimetric scale.

Chronology

The chronology of core TSR-18-I was established by correlation with the previously ^{210}Pb dated core TSR-17-I (Halac *et al.*, 2020). Both cores, TSR-18-I and TSR-17-I, were correlated based on the magnetic susceptibility pattern, water content depth-profile values and according to sedimentary features (Fig. 2). ^{210}Pb age-depth model of core TSR-17-I has been published elsewhere (Halac *et al.*, 2020).

Pigment analysis

Pigment analyses were performed at the High Performance Liquid Chromatography Laboratory (CEPROCOR, Córdoba, Argentina) on samples taken

every 1 cm, according to the method described by Lami *et al.* (1994). Pigments in samples of ≈ 1 g wet sediment were extracted overnight with 10 mL of acetone/water mixture (90:10), under nitrogen atmosphere and maintained at $4^\circ C$ in darkness. The extracts were vortexed and centrifuged at 3,000 g for 10 min. The supernatant was filtered through a Durapore (PVDF) filter ($0.22 \mu m$ diameter) and the extraction was repeated (2 to 3 times) until the supernatant was colorless. Chlorophyll derivatives (CD) and total carotenoids (TC) were measured in a visible UV spectrophotometer (UV-160 Shimadzu) with a 1-cm light pass cuvette. The extracts were read at 410, 430, 450, 665, and 750 nm. Carotenoid concentrations were expressed in $mg \cdot g^{-1}$ organic matter ($mg \cdot g^{-1}$ LOI) (Züllig, 1985), whereas chlorophyll derivatives were expressed in absorbance units (U) per g of organic matter ($U \cdot g^{-1}$ LOI), (Guilizzoni *et al.*, 1983). Individual carotenoids and chlorophylls were detected by Reversed Phase High-Performance Liquid Chromatography with a Photodiode Array Detector (Alliance 2690 and 996 PDA, Waters). The gradient elution program was performed according to Lami *et al.* (2000) in a C18 column (Phenomex C18 Luna $5 \mu m$ particle size; 250 mm x 4.6 mm ID). The pigments isolated from sediments were identified by spectral comparison (between 400 and 670 nm) and retention time (Rt) with those obtained for commercial pigment standards (DHL Laboratory Products, Denmark). Chromatograms were extracted at 460 and 665 nm. The concentration of carotenoids and chlorophylls (and their derivatives) was expressed in terms of organic matter (LOI at $550^\circ C$) to take pigment degradation into account (Hodgson *et al.*, 2004). The concentration of pigments was determined on the basis of molar extinction coefficients at detection wavelengths. The molar extinction coefficients $E1\% 460$ and $E1\% 656$ were derived from the $E1\% \max$ reported in Egeland *et al.* (2011). The pigment affiliation was based on Guilizzoni and Lami (2003).

Urban growth analysis

Spatio-temporal urban growth analysis in the SRr catchment area was based on a multi-temporal analysis of Landsat 5 (1987, 1997, 2007) and Landsat 8 (2017) satellite images. This analysis was performed with the SNAP software (version 7.0.0) by unsupervised K-means cluster analysis. Clusters

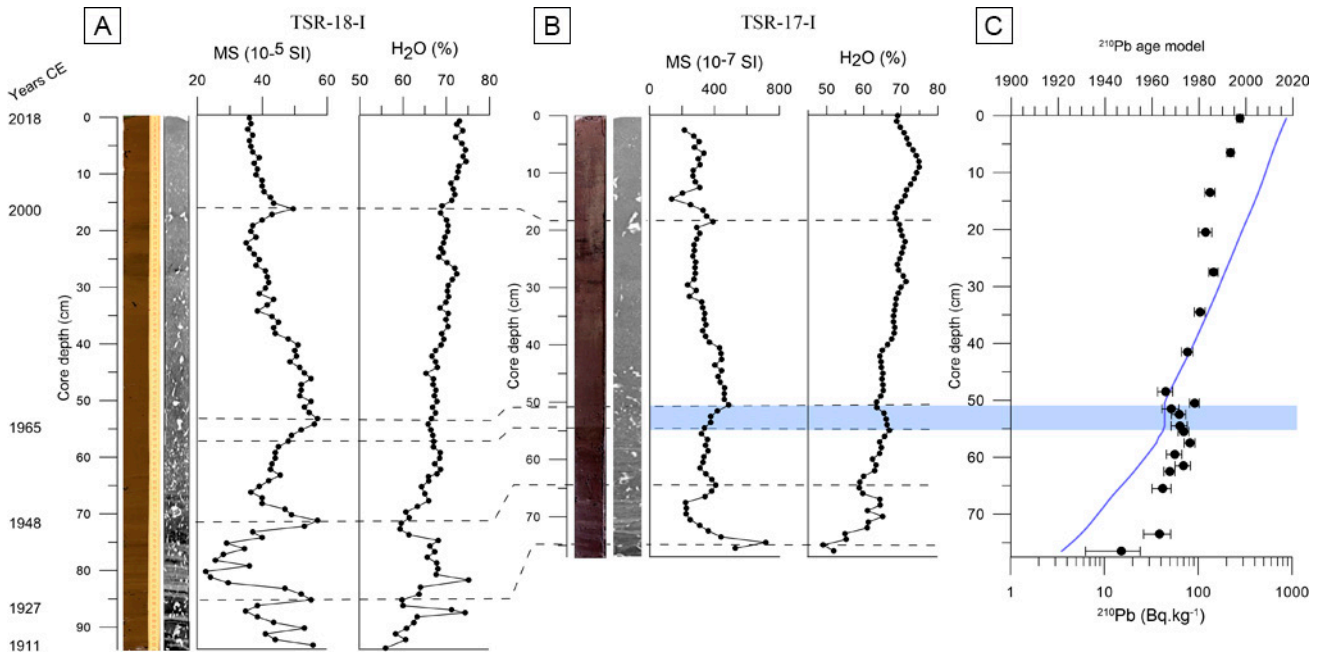


Figure 2. a) and b) Magnetic susceptibility (MS, 10^{-5} SI units) and water content (H_2O , %) of TSR-17-I and TSR-18-I, respectively. c) ^{210}Pb age model of TSR-17-I (Halac *et al.*, 2020). Correlation of maximum and minimum values of the proxies between both cores is shown by broken lines. The light-blue band indicates the levels of TSR-17-I (55–51 cm) assigned to 1965 CE.

corresponding to urban areas were added to each image to determine the total urban area at different years, using the equation (1). The estimation of interdecadal urban growth was expressed as a percentage.

$$\text{Urban area (km}^2\text{)} = \left(\frac{\sum \text{urban area clusters (\%)}}{\text{total area (km}^2\text{)}} \right) \times 100 \quad \text{eq. (1)}$$

Statistical analysis

A constrained hierarchical cluster analysis (CONISS) and the broken stick model, performed with the Rioja package (Juggins, 2009; R software), were used to statistically confirm sedimentary facies previously outlined along core TSR-18-I (see Sedimentary facies). This analysis made it possible to recognize distinctive portions of sediments based on measured proxies (SM, TOC, TIC, DC and CT). Furthermore, Principal Component Analysis (PCA; Oksanen *et al.*, 2019; Vegan package, R software) was further performed to inspect proxy relationship and variation patterns along the sedimentary record. Before applying PCA, the linear response of analyzed proxies was confirmed (Jongman *et al.*, 1995).

Total annual precipitation (mm) (at 31.25° S, 64.25° W) for the period 1901–2018 CE was obtained from CRU TS 4.04 dataset $0.5^\circ \times 0.5^\circ$ cell series

(Harris *et al.*, 2020). Annual precipitations were calculated according to the hydrological year of the region (July yr^1 to June yr^{+1}).

RESULTS

Age model

Cores TSR-18-I and TSR-17-I were correlated based on the presence of sedimentary structures and according to the magnetic susceptibility pattern and water content values at four distinctive levels along core-depth (see Fig. 2 and Table 1). The presence of thick lamination, maximum values of MS (55×10^{-5} and 716×10^{-7} SI in TSR-18-I and TSR-17-I, respectively), and minimum values of H_2O (60 and 55% in TSR-18-I and TSR-17-I) at level 86 cm in core TSR-18-I allowed to link this section with level 75 cm in core TSR-17-I (Fig. 2a, b). According to the ^{210}Pb age model developed in TSR-17-I, level 75 cm corresponds to 1927 CE (Fig. 2b). Ages below level 86 cm were extrapolated based on the sedimentation rate value estimated in the basal section of TSR-17-I (0.49 cm. yr^{-1}). Thus, an age of 1911 CE was assigned to the TSR-18-I base (level 94 cm; Fig. 2a, b).

Another correlation was established between levels 72 cm (core TSR-18-I) and 65 cm (core TSR-

17-I). The development of laminated sediments and an increase in MS values at level 72 cm (core TSR-18-I) can be correlated with a shift in MS value in laminated sediments at level 65 cm on TSR-17-I. According to Halac *et al.* (2020), level 65 cm corresponds to 1948 CE (Fig. 2a, b). The shift toward higher MS values identified between levels 58–54 cm in TSR-18-I and 55–51 cm in TSR-17-I, make it possible to correlate both intervals and to assign a ²¹⁰Pb age of 1965 CE (Fig. 2). A constant decreasing pattern of MS values and an increase in H₂O values occur upwards, from levels 54 cm (core TSR-18-I) and 51 cm (core TSR-17-I) up to levels 17 cm and 19 cm respectively, where MS values display a marked peak. Then, the assigned ²¹⁰Pb age for level 17 cm in TSR-18-I is 2000 CE (Fig. 2a, b). The core correlation in these intervals is strengthened by the presence of faintly laminated muds at 28–24 cm/ 22–19 cm in TSR-18-I and at 30–29 cm and 25–11 cm in TSR-17-I (Fig. 2a, b).

General core description

Multi-proxy features, including sedimentology, geochemistry, and pigment data of core TSR 18-I, are presented in figures 3 and 4. Sediments overall core TSR-18-I correspond to a succession of dark brown to black banded, laminated to faintly laminated and massive muds. Laminated silty-sandy sediments are present in the core basal portion (between levels 83.5–74.5 cm). Magnetic susceptibility values range between 23 and 57 * 10⁻⁵ SI with maximum values along the lowermost section of the core. H₂O varies between 56 and 75%, with an increasing trend towards the top of the core. Relative density values range from 0.33 to 0.79 g.cm⁻³, which maximum values along the lowermost section followed by a decreasing trend toward the top of core. Relative density curve match magnetic susceptibility variability and mirror H₂O values.

Total inorganic carbon (TIC) and total organic carbon (TOC) percentages vary from 1.1 to 3.4% and 4.4 to 6.8%, respectively. Both proxies exhibit comparatively higher values at the base of the core followed by a decreasing trend along the middle section (from level 60 to level 12 cm) and an increment toward the top of the core, where they reach the maximum TOC values.

Total carotene (TC) values range from 0.3 to 1.5 mg. g LOI⁻¹, presenting maximum values at the

TSR-18-I level (cm)	TSR-17-I level (cm)	²¹⁰ Pb age (CE)
86	75	1927
72	65	1948
58-54	55-51	1965
17	19	2000

Table 1. Correlated levels between TSR-17-I and TSR-18-I and associated ages.

core bottom, followed by a steady upward decrease. Chlorophyll derivative (CD) values vary from 16 to 149 U_g. g LOI⁻¹, showing a steady increase from base to top, where the maximum values are observed.

Seven lithological units (LU; Fig. 3) were distinguished along the core based on sedimentary structures, texture, type of contacts and color of sediments as well as by physical and chemical proxies (TOC, TIC, TC and CD). A general description with mean values of measured proxies is presented in table 2.

Sedimentary facies

Following the criteria proposed by the Limnological Research Center Core (<http://lrc.geo.umn.edu/lacore/icd.html>) and according to Schnurrenberger *et al.* (2003), the identified lithological units (Table 2) were merged into four sedimentary facies (D, C, B and A). The proposed facies scheme was further confirmed by a cluster analysis CONISS and the broken stick model (Figs. 3, 4).

Facies D (94–64 cm) includes LU 1, 2, and 3. It is composed of gray to dark brown silty-sandy to muddy sediments. This facies is mostly massive, except for the laminated to banded interval from levels 83.5 to 75.5 cm (Table 2). MS, relative density, TC and TOC present a very variable pattern (MS: 22-57 * 10⁻⁵ SI, mean value: 41 * 10⁻⁵ SI; relative density: 0.33-0.79 g.cm⁻³, mean value: 0.56 g.cm⁻³; TC: 0.3– 1.5 mg. g LOI⁻¹, mean value: 0.7 mg. g LOI⁻¹; TOC: 4.7–6.1%, mean value: 5.3%) while H₂O, CD and TIC exhibit the lowest values of the entire record (H₂O: 56–64%, mean value: 75%; CD: 16–70 U_g g LOI⁻¹, mean value: 32 U_g. g LOI⁻¹; TIC: 1.1–3.1%, mean value: 2.0%) (Figs. 3, 4). Regarding high MS variability, facies

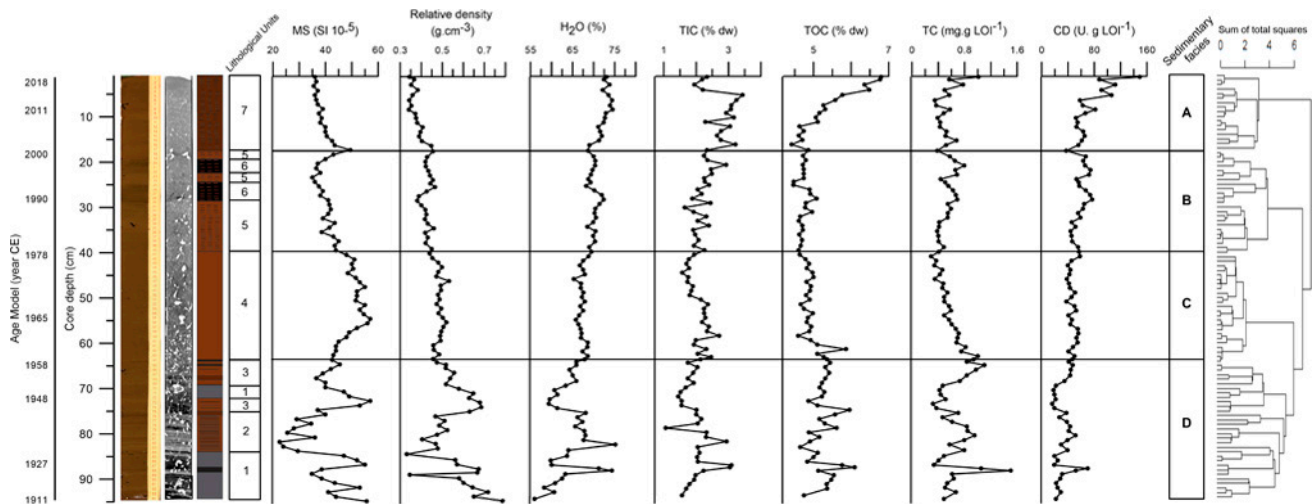


Figure 3. Depth profiles of physicochemical and biological proxies in the SRr core (TSR-18-I): magnetic susceptibility (MS, 10^{-5} SI units), relative density ($\text{g}\cdot\text{cm}^{-3}$), water content (H_2O , %), total inorganic carbon (TIC, %), total organic carbon (TOC, %), total carotenes (TC, $\text{mg}\cdot\text{g LOI}^{-1}$) chlorophyll derivatives (CD, $\text{U}\cdot\text{g LOI}^{-1}$). Core photograph, computed tomography image and lithological units are shown on the left. Sedimentary facies D, C, B and A are indicated from base to top. Cluster analysis is shown on the right and matches with sedimentary facies.

D presents several MS peaks (86–84 cm and 73–71 cm) coincident with the development of laminated sandy-silts as well as a drop in the MS values (90–85 cm and 83–74 cm) simultaneously to the increment of organic matter proxies.

Facies C (64–40 cm) is composed of massive dark brown muds (LU 4). One of the main features of facies C is the development of 4-mm-thick black laminae (Fig. 4, level 64 cm). In general, MS, relative density, and H_2O present a lower variability than in facies D (e.g. MS values range between 42 and $57 \cdot 10^{-5}$ SI; relative density between $0.46\text{--}0.53\text{g}\cdot\text{cm}^{-3}$; and H_2O between 65 and 68%). Relative density presents a lower mean value in comparison with facies D (from 0.56 to $0.49\text{g}\cdot\text{cm}^{-3}$). TOC (mean value: 4.9%, maximum value: 5.9%) and TC (mean value: $0.6\text{mg}\cdot\text{g LOI}^{-1}$, maximum value: $1.0\text{mg}\cdot\text{g LOI}^{-1}$) show lower values than facies D. Moreover, facies C is characterized by a marked decreasing trend of TC from base to top. CD values range between 38 and $56\text{U}\cdot\text{g LOI}^{-1}$ (Figs. 3, 4).

Facies B (40–18 cm) comprises LU 5 and 6 and is composed of dark brown to black massive/faintly laminated muds (Table 2). The basal contact with facies C is diffuse. MS and relative density values show a decreasing pattern (48 to $35 \cdot 10^{-5}$ SI; 0.47 to $0.38\text{g}\cdot\text{cm}^{-3}$) (Figs. 3, 4). Some organic proxies display an upward increasing trend along facies B, exhibiting comparatively higher mean values than

in facies C (TIC: mean value 2.2%, maximum value 2.9%; CD: mean value $59\text{U}\cdot\text{g LOI}^{-1}$, maximum value $77\text{U}\cdot\text{g LOI}^{-1}$). Conversely, TC and TOC show a uniform pattern.

Facies A (18–0 cm) includes LU 7 and consists of very dark brown weakly laminated muds. The basal portion of this facies is marked by a sharp increment in the MS value while there is a noticeable upward decrease in H_2O , TIC, TOC, TC and CD values. Along the uppermost portion of the core this facies shows a marked change toward higher values in the organic proxies (TOC: mean value 6.3%, maximum value 6.8%; TC: mean value $0.5\text{mg}\cdot\text{g LOI}^{-1}$, maximum value $1.0\text{mg}\cdot\text{g LOI}^{-1}$ and CD: mean value $73\text{U}\cdot\text{g LOI}^{-1}$, maximum value $149\text{U}\cdot\text{g LOI}^{-1}$). Furthermore, TOC and CD reach the maximum values of the entire core at the uppermost sediments, while MS and relative density exhibit the minimum values of the core (Table 2).

Multi proxy data ordination

PCA analysis on the multi proxy data (Table 3) showed that two main components (PC1 and PC2) account for a total of 66.6% of the total variance (42 and 24.6%, respectively). The aggrupation of samples according to the identified facies becomes evident in Fig 5. PC1 shows a significant positive correlation with MS, and a negative correlation

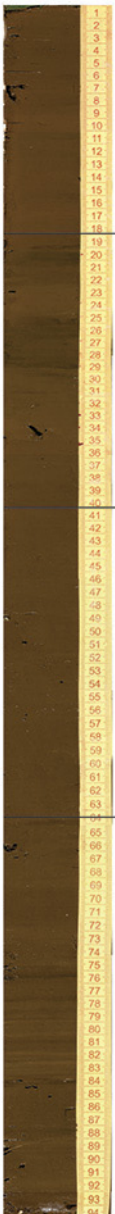
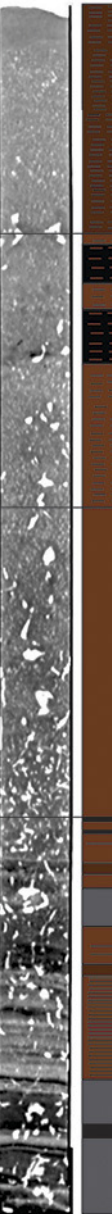

Photograph, tomography, and scheme of TSR-18-I			Sedimentary facies description	
Depth (cm) 0 1 2 3 4 5 6 7 8 9 10 11 12 13 14 15 16 17 18 19 20 21 22 23 24 25 26 27 28 29 30 31 32 33 34 35 36 37 38 39 40 41 42 43 44 45 46 47 48 49 50 51 52 53 54 55 56 57 58 59 60 61 62 63 64 65 66 67 68 69 70 71 72 73 74 75 76 77 78 79 80 81 82 83 84 85 86 87 88 89 90 91 92 93 94				FA Weakly laminated muds. Very dark brown mud . MS 35- 49 *10 ⁻⁵ SI H ₂ O 69-74 % TC 0.3-1.0 mg.g LOI ⁻¹ TIC 1.9-3.4 % DC 37- 149 Ug.g LOI ⁻¹ TOC 4.4-6.8 % relative density 0.34-0.46 g.cm ⁻³
	FB Weakly laminated muds. Black to dark brown mud. MS 35- 48 *10 ⁻⁵ SI H ₂ O 68-72 % TC 0.3- 0.8 mg.g LOI ⁻¹ TIC 1.6-2.9 % DC 45- 77 Ug.g LOI ⁻¹ TOC 4.5-5.1 % relative density 0.38-0.47 g.cm ⁻³			
	FC Massive muds. Brown mud. MS 42-57 *10 ⁻⁵ SI H ₂ O 65-69 % TC 0.34-1.0 mg.g LOI ⁻¹ TIC 1.6-2.7 % DC 38-56 Ug.g LOI ⁻¹ TOC 4.6-5.9 % relative density 0.46-0.53 g.cm ⁻³			
	FD Laminated to massive silty clayey to silty-sandy sediments. Gray to dark brown sediments. MS 22- 57 * 10 ⁻⁵ SI H ₂ O 56-75 % TC 0.3- 1.5 mg.g LOI ⁻¹ TIC 1.1-3.1 % DC 16- 70 Ug.g LOI ⁻¹ TOC 4.7-6.1 % relative density 0.33-0.79 g.cm ⁻³			

Figure 4. Description of sedimentary facies including: value range of the main proxies (MS, relativedensity, H₂O, TIC, TOC, TC, and CD; see abbreviations in figure 3), core photograph, computed tomography image and lithological unit scheme of TSR-18-I.

with organic proxies (Table 3). Most of the samples corresponding to facies D and facies C are positively related, while samples of facies A are negatively associated with PC1; samples of facies B are located in the central area of PC1 (Fig. 5). Regarding PC2, there is a significant positive correlation with TOC and TC, and a negative one with TIC and CD (Table 3). In general, samples of facies D are positively associated, while most samples of facies C, B, and A are negatively related to PC2 (Fig. 5).

Fossil pigments

Figure 6 shows the values of chlorophyll-*a* (chl *a*) and their derivatives, and βcarotene along TSR-18-I core. Chl *a* was detected in facies A and B, and along some intervals of facies D, reaching its maximum values in facies A (26 and 21 nmol.g LOI⁻¹). Pheophytin *a* (pheo *a*) is mostly constant throughout the record, except in facies B where the highest values are present (*e.g.*, 340, 274, 230 nmol.g LOI⁻¹).

Pheophorbide *a* (pheide *a*) shows a constant upward increase along the core, reaching its highest values in facies A (e.g., 412, 411, 380 nmol. g LOI⁻¹; levels 3, 2 and 5 cm, respectively). The highest values of pheide *a* and chl *a* at the uppermost section mostly account for the CD increase at the core top (Figs. 3, 6). β -carotene ($\beta\beta$ -car) presents great variability throughout the core (183–6234 nmol. g LOI⁻¹), while the highest values are present in facies D. This pattern is also shown by TC along facies D (Figs. 3, 6). $\beta\beta$ -car decreases upwards, until it reaches non-detectable values in the uppermost portion of facies A.

DISCUSSION

The multi-proxy analysis of the sedimentary core TSR-18-I provided the basis for reconstructing changes in the environmental condition of the SRr during the period from 1911 to 2018 CE. The combined analysis of sedimentary facies, geochemistry and fossil pigments throughout the paleolimnological record made it possible to decipher four stages in the SRr based on temporal changes in sedimentation, organic matter sources and the trophic states of the reservoir. The analysis of hydrometeorological and land use data provided clues to unravel the influence between natural and/or anthropic drivers of recorded environmental changes.

Multiproxy reconstruction of environmental changes in the SRr

MS value variations throughout the record (Fig. 3) indicate changes in lake sediment composition, which may be controlled by the dynamics of the fluvial input over time (e.g., Brahney *et al.*, 2008; Menounos, 1997). In a low water volume scenario, higher fluvial influence at the inner-lake is recorded by laminated sandy sediments characterized by high values of MS and relative density (facies D and C). Conversely, finer sediments and a decreasing trend of MS and relative density can be associated with dominant pelagic sedimentation in a water body with larger volume, which would have conditioned the transport of coarser sediments from the tributary rivers to the inner-lake area (facies B and A). The distinctive patterns of sedimentary dynamic ruled by the changes in the water column depth are reflected by the PCA1, which correlates highly with MS values. Facies D and C (high MS values) can be

associated with sedimentation under comparatively lower water levels, while facies B and A (low MS values) with the settling of particles at a larger column of water (Fig. 5 and Table 3).

Primary production proxies (TC and CD) allowed to track changes in the sedimentary organic matter source, reflecting a temporal shift from a terrestrial plant-dominated delivery (high TC content) to a phytoplankton-dominated state (high CD content). Previous studies demonstrated that carotenes (TC) are more closely associated with vascular plants (either terrestrial or macrophytes) than with phytoplankton (Carpenter and Leavitt, 1991). Since carotenes degrade more slowly than chlorophyll-*a* (chl *a*) and its derivatives (phe *a*, pheide *a*), they better preserve the signal of littoral and terrestrial contributions (Carpenter and Leavitt, 1991). In addition, carotenes are more easily degraded by grazing since they are fully metabolized. Conversely, chlorophylls derived from predated phytoplankton are converted into derivative composites like pheophorbides (i.e. pheide *a*) (Leavitt, 1993).

Regarding the dominant source of the sedimentary organic matter, PC2 can be used to better distinguish main changes in the dominant source for each facies. Positive correlation of PC2 with TC confirms the prevalence of a terrestrial source of OM during the deposition of facies D, from 1911 to 1958 CE. Conversely, the negative correlation of PC2 with CD and TIC, both with high values in facies B (from 1978 to 2000 CE) and A (from 2000 to 2018 CE), and in a larger proportion of facies C, is in agreement with an important change to a dominant autochthonous origin of the organic matter. The positive correlation between CD and TIC would highlight the biogenic control on the precipitation of carbonates. High pelagic primary production may trigger the precipitation of carbonates (Thompson *et al.*, 1997) during cyanobacteria blooms (Teranes *et al.*, 1999; Obst *et al.*, 2009). Thus, high TIC values would indicate a high primary production condition, as it increases during algal blooms events. Therefore, in our study, facies D can be linked to an important input of organic matter derived from littoral plants, while facies B, A and a broad proportion of facies C, to a dominant pelagic primary production (Fig. 5).

Stage 1 (94–64 cm/1911–1958 CE)

This stage characterizes the initial condition of

L. Unit (LU)	Depth (cm)	Description	Mean values (proxies)	
1	94.0-83.5 71.5-68.5	Dark to very dark gray, massive silts to sandy silts.	MS = 47 * 10 ⁻⁵ SI TIC = 1.9 % TOC = 5.3 % relative density = 0.63 g.cm ⁻³	H ₂ O = 62 % TC = 0.6 mg. g LOI ⁻¹ CD = 26 Ug. g LOI ⁻¹
2	83.5-75.5	Dark brown, laminated muds (dark laminae: 2 to 4 mm. Sharp and planar basal contact. The top is gradational towards unit 3.	MS = 31* 10 ⁻⁵ SI TIC = 2.2 % TOC = 5.2 % relative density = 0.47 g.cm ⁻³	H ₂ O = 68 % TC = 0.8 mg. g LOI ⁻¹ CD = 41 Ug. g LOI ⁻¹
3	75.5-71.5; 68.5-63.5	Dark brown banded to faintly laminated muds. Dark bands ranges between 1-1,5 cm thick and laminations from 1 to 3 mm thick. The top is gradational to unit 4.	MS = 40 * 10 ⁻⁵ SI TIC = 1.9 % TOC = 5.4 % relative density = 0.55 g.cm ⁻³	H ₂ O = 65 % TC = 0.7 mg. g LOI ⁻¹ CD = 33 Ug. g LOI ⁻¹
4	63.5-40.0	Dark brown massive muds. The top is gradational to unit 5.	MS = 50 * 10 ⁻⁵ SI TIC = 2.1 % TOC = 4.9 % relative density = 0.49 g.cm ⁻³	H ₂ O = 67 % TC = 0.6 mg. g LOI ⁻¹ CD = 46 Ug. g LOI ⁻¹
5	40.0-28.0; 24.0-22.0; 19.0-18.0	Dark brown faintly laminated muds. Dark laminae: 1 to 2 mm thick. The top is gradational to unit 6.	MS = 41 * 10 ⁻⁵ SI TIC = 2.1 % TOC = 4.7 % relative density = 0.43 g.cm ⁻³	H ₂ O = 70 % TC = 0.5 mg. g LOI ⁻¹ CD = 54 Ug. g LOI ⁻¹
6	28.0-24.0; 22.0-19.0	Black weakly laminated muds. Laminae: 1 to 2 mm thick. Gradational contact towards unit 7.	MS = 38 * 10 ⁻⁵ SI TIC = 2.3 % TOC = 4.8 % relative density = 0.42 g.cm ⁻³	H ₂ O = 70 % TC = 0.7 mg. g LOI ⁻¹ CD = 70 Ug. g LOI ⁻¹
7	18.0-0.0	Very dark brown weakly laminated muds. Dark laminae: up to 1 mm thick.	MS = 39 * 10 ⁻⁵ SI TIC = 2.7 % TOC = 5.4 % relative density = 0.38 g.cm ⁻³	H ₂ O = 72 % TC = 0.5 mg. g LOI ⁻¹ CD = 73 Ug. g LOI ⁻¹

Table 2. Description of the lithological units (LU), and mean values of proxies (MS: Magnetic Susceptibility; H₂O: Sediment Water Content; TIC: Total Inorganic Carbon; TOC: Total Organic Carbon; TC: Total Carotenes; CD: Chlorophyll Derivatives).

the water body after the construction of the first SRr dam (foundation) and the infilling process during its last part after the second dam building. The corresponding record (facies D) can be well differentiated due to the large variability in sediment composition and physiochemical proxies (MS: 22–57 * 10⁻⁵ SI; relative density: 0.33-0.79 g.cm⁻³; H₂O: 56–75.1%; TOC: 4.7–6.1%). High MS values and coarser sediments (silt-sandy laminae) indicate the occurrence of episodic periods of high river influence (i.e.: 86–84 cm, 1926–1929 CE/73–71 cm, 1946– 1949 CE). Indeed, the presence of coarse-grain fluvial sediments was highly favored due to the lower water-volume. In particular, the short periods of highest river influence are coeval with a diminished

primary lake production (i.e.: precipitation increase and CD decrease; Fig. 7).

The decrease of MS and rise of organic proxies in the record of stage I (TOC: mean values 5.4%, TC: mean values 0.8 mg.g LOI⁻¹) (90–85 cm, 1918–1925 CE/83–74 cm, 1931–1945 CE) can be linked to a minor fluvial contribution and thus, to a lower reservoir volume which promote the development of a littoral biota. Previous results (Cachi, 1975; Gavilan, 1981) report that prolonged low volume periods favored the growth of littoral plant communities around the SRr. These plant communities were submerged during periods of increased volume, becoming part of the input of organic matter into the system.

Overall, the low content of CD and pheide *a* in the

	PC 1	<i>p</i> -value	PC 2	<i>p</i> -value
TC	-0.71	< 0.001	0.35	< 0.001
CD	-0.72	< 0.001	-0.43	< 0.001
TOC	-0.52	< 0.001	0.65	< 0.001
TIC	-0.56	< 0.001	-0.69	< 0.001
MS	0.70	< 0.001	-0.15	n/s

Table 3. Correlation coefficients among proxies (MS, TOC, TIC, CT, DC; see abbreviations in figure 3) and PCA axes and their *p*-values. Number of samples: 94.

record of stage I (mean: 32 U_g.g LOI⁻¹ and 31 nmol.g LOI⁻¹, respectively) indicates low autochthonous primary production in comparison with the following stages (see Fig 6 and 7), probably due to a combined effect of low nutrient input, water column instability and turbidity (Halac *et al.*, 2020). It is known that the mentioned factors are detrimental to the development of phytoplankton communities (e.g., Dokulil, 1994; Liu *et al.*, 2011).

Low precipitations (annual mean: 624 mm) characterized hydroclimatic conditions during stage 1 (1901–1958 CE), resulting in frequent reservoir volume fluctuations during prolonged drought events. This is in agreement with the hydroclimatic variability observed in central Argentina, where frequent drought events were registered during the first half of the 20th century. In particular, a specific period of severe droughts was identified in the 1930s in the Pampean region, known as the “Dust Bowl Drought,” which was characterized by extremely arid conditions, soil erosion and dust storms (Tripaldi *et al.*, 2013; Guerra *et al.*, 2015, 2016).

Stage 2 (64–40 cm/1958–1978 CE)

A second stage characterized by new environmental conditions in the SRr was the result of the noticeable increase in water volume and stabilization of the water column after the second dam was built (Fig. 7). Stage 2 is mostly recorded by massive and homogenous sediments (Facies C), which would indicate pelagic sedimentation in a deeper water column overall the inner lake (Renaut and Gierlowski-Kodersch, 2010).

The onset of stage 2 is marked by an increase of TOC and TC values and a decreasing trend in relative density, probably due to pulses of terrestrial organic matter delivery caused by the water inflow after the second dam was built during the last part of stage 1 (Fig. 7b; *c.a.* 1944–1952 CE). The SRr volume increase from 91 hm³ in 1947 CE to 144 hm³ in 1952 CE (Stage 1; Fig. 7b), promote the expansion of the inner-lake area (lacustrine zone) recorded at the end of stage 1 and the onset of stage 2. A larger lake volume resulted in a new lake base level, a migration of the shore-line and thus the mobility of river mouths. TOC and TC values decreased steeply upwards (Fig. 3), which would reflect a diminished input of organic matter derived from littoral plants. In addition, the maintenance of low values of DC would indicate a low autochthonous primary production. Conditions of low productivity after periods of water infilling have also been reported in other reservoirs, since a non-equilibrium trophic condition, due to the nutrient depletion, would trigger a drop in primary production (Turgeon *et al.*, 2016).

The record of the last part of stage 2 includes the effect of the largest recorded hydroclimatic jump occurred after the mid-1970s, due to a change in the South American Monsoon System’s (SAMS) activity. This event resulted in an increase in precipitation in the Southeast South American (SESA) region (Compagnucci *et al.*, 2002; Piovano *et al.*, 2004, 2009; Pasquini *et al.*, 2006; Garreaud, 2009; Troin *et al.*, 2010). Moreover, many studies reported a direct relationship between the positive phase of El Niño-South Oscillation (ENSO) and the increase of summer precipitation, intensified as of the beginning of 1970s (Camilloni and Barros, 2003; Troin *et al.*, 2016; Guerra *et al.*, 2018). The instrumental record shows the synchronous rise of the total annual precipitation (mean value: 736 mm; 1959–2018 CE) and the annual mean of the SRr’s volume as of the 1970s (Fig. 7a, b).

Stage 3 (40–18 cm/1978–2000 CE)

Stage 3, recorded by facies B, corresponds to conditions during the period from 1978 to 2000 CE. The decrease of MS values (mean value: 40 * 10⁻⁵ SI) indicates particle settling in a well-developed pelagic zone, while higher values of CD (maximum value: 77 nmol.g LOI⁻¹), phaeo *a* (maximum value:

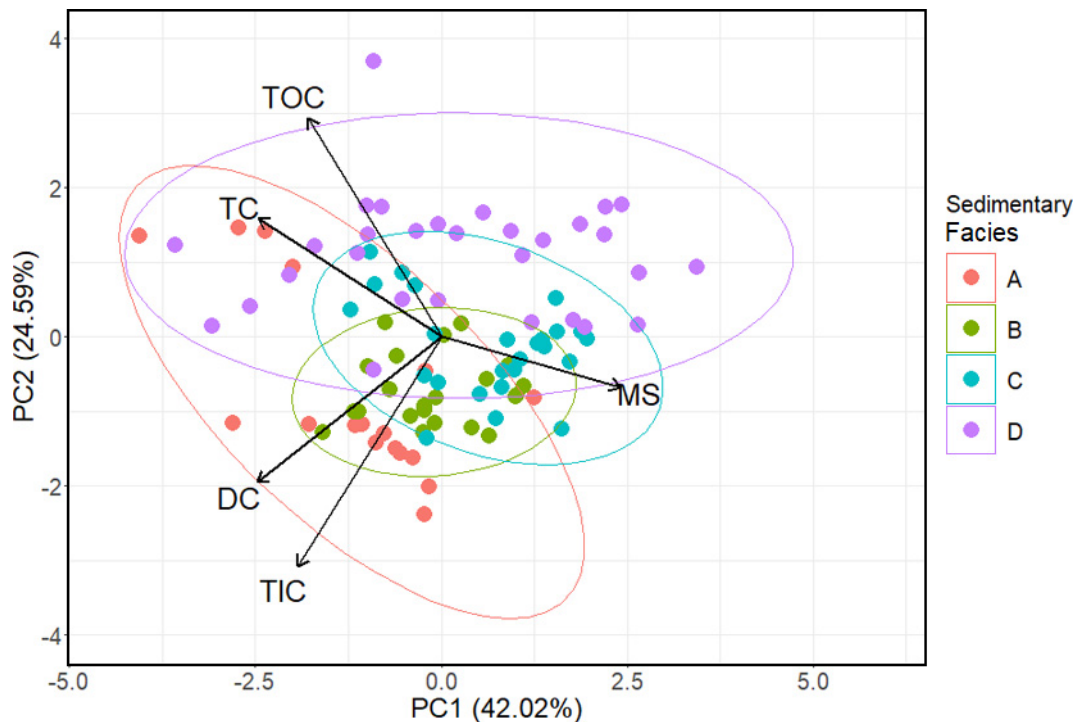


Figure 5. Principal Component Analysis biplot. Data set includes: MS, TIC, TOC, TC, and CD (see abbreviations in figure 3). The first axis, PC1, is positively correlated with MS, and the second axis, PC2, is positively correlated with TOC and TC, and negatively correlated with TIC and DC. The samples are grouped according to sedimentary facies.

341 nmol.g LOI⁻¹), chl *a* (maximum value: 26 nmol.g LOI⁻¹) and pheide *a* (maximum value: 304 nmol.g LOI⁻¹) reflect an increase in autochthonous primary production in comparison to previous stages, associated with a major development of phytoplankton communities. Regarding the increase of TC (maximum value: 0.8 mg.g LOI⁻¹) during stage 3, it could be attributed to the increase of specific carotenes derived from some phytoplankton groups (e.g., echinone, canthaxanthin, diatoxanthin; Halac *et al.*, 2020). In addition, the synchronic increase of pheide *a* and TIC would reinforce that higher precipitation of carbonates may be a response to the increment of phytoplankton communities. The presence of dark bands in facies B (28–24 cm/22–19 cm in Fig. 4) would confirm conditions of high primary production.

In agreement with our results, limnological studies through the decades of 70s and 80s identified a eutrophic state for the SRr and a growth of phytoplankton communities during warm seasons (García de Emiliani, 1977; Gavilan, 1981; Prospero, 1986). Thus, the autochthonous organic matter increase recorded in sediments might have been caused by external nutrient load

increases which would indicate an intensification of the eutrophication process. Considering that the hydroclimate condition was similar to those during Stage 2, the main factor influencing a higher nutrient input to the SRr could be attributed to the population increase in the catchment since ~1960 CE (i.e., due to sewage effluents increase). According to census data, the population of the city of Villa Carlos Paz increased by 300% during the period 1947–1960 CE, and up to 900% from 1960 to 2001 CE (<https://www.indec.gov.ar/indec/web/InstitucionalIndec-BibliotecaEnLinea>).

In addition, during stage 3, the population increase was probably promoted by changes in water management policies that diminished the “boundary level allowed for urbanization” in the SRr littoral area by -2 m (provincial decree No. 8178; <http://agrimensorescordoba.org.ar/documentos/decreto-prov-no-817869-cota-36-38carlos-paz.pdf>). The latter allowed to increase the available area for urbanization around the SRr. Moreover, after the 70s, the temporal population during the tourist season grew to three times the permanent population (Gavilán, 1981; <https://biblioteca.indec.gov.ar/bases/minde/1c1980b5.pdf>).

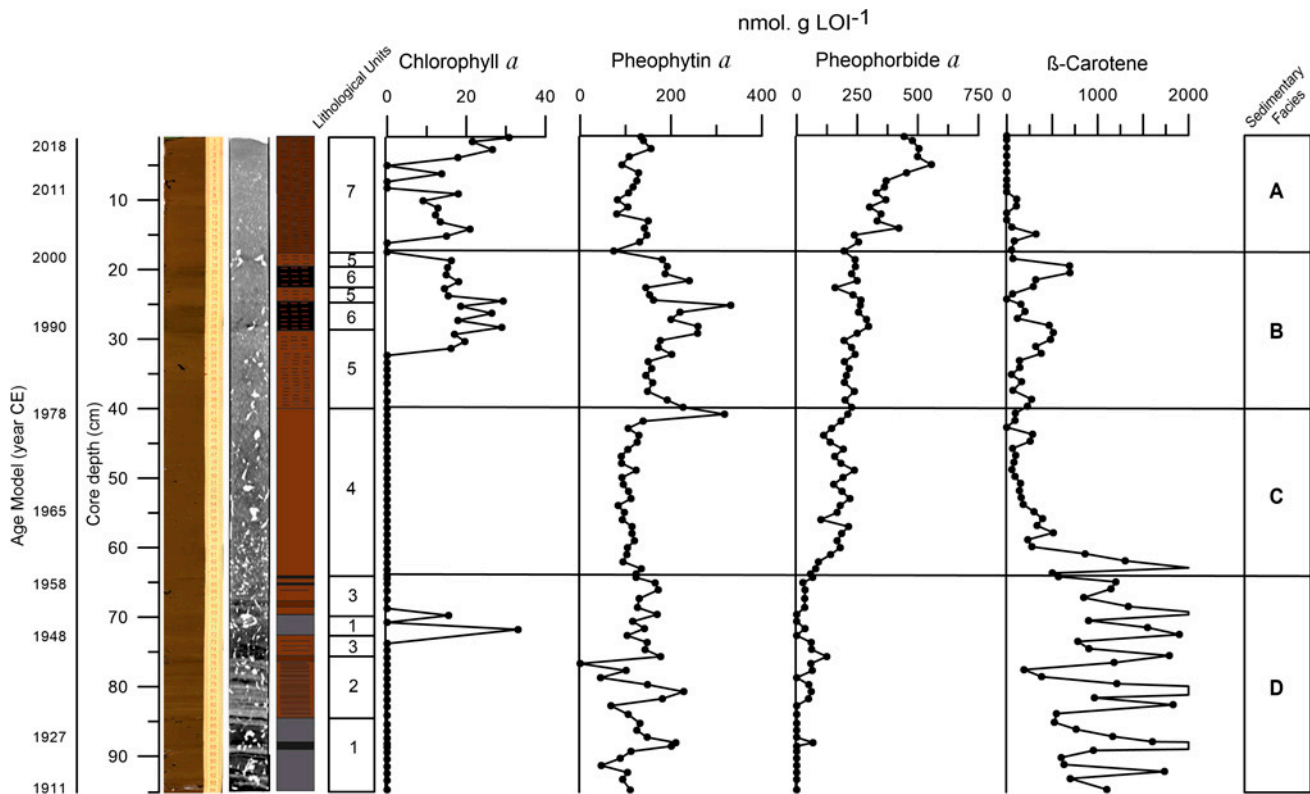


Figure 6. Depth profiles of fossil pigments: chlorophyll-*a* (chl *a*), pheophytin *a* (pheo *a*), pheophorbide *a* (phide *a*), and β -carotene ($\beta\beta$ -car) (nmol.g LOI^{-1}). Sedimentary facies D, C, B and A are indicated from base to top. Core photograph, computed tomography image, and lithological units are shown on the left.

Stage 4 (18–0 cm/2000–2018 CE)

Stage 4 is represented by facies A, and corresponds to the period from 2000 to 2018 CE. This stage can be distinguished by an abrupt and synchronic increase of all organic proxies, which displayed the highest values along the record (e.g. TOC: maximum value: 5.3%, CD: maximum value $149 \text{ Ug.g LOI}^{-1}$, TC: maximum value $1.0 \text{ mg.g LOI}^{-1}$, chl *a*: maximum value $26 \text{ nmol.g LOI}^{-1}$, pheide *a*: maximum value $485 \text{ nmol.g LOI}^{-1}$ and TIC: maximum value 3.4%; Figs. 3, 6), reflecting the acceleration of the eutrophication process. According to our results, contemporary SRr monitoring during 2006–2016 CE (Rodríguez and Ruiz, 2016) show that an increase in nutrient concentration in the water column (mainly phosphorus and nitrogen) caused a shift from eutrophic to hypereutrophic conditions during stage 4. As a consequence, frequent events of summer algal blooms led to a condition of deep-water anoxia which promoted the release of nutrients from lake bottom sediments. Therefore, nutrients stored in the sediments of the SRr would represent an important

internal supply (Rodríguez and Ruiz, 2016; Halac *et al.*, 2019; Pussetto *et al.*, 2020).

The acceleration of the SRr eutrophication process, reflected both by sedimentary organic proxies and the contemporary monitoring data, is probably a consequence of the marked increase in population in the city of Carlos Paz and throughout the basin during the period 2001–2020 CE (~20% and ~40%, respectively <https://www.indec.gov.ar/indec/web/Nivel4-Tema-2-41-135>) and a growth in tourists number (5 times more than the permanent population in January during CE 2010–2017; <https://datosestadistica.cba.gov.ar/dataset/sector-turismo>).

CONCLUSIONS

The paleolimnological record of the SRr provides a detailed archive of the environmental changes that occurred during the 20th and 21st centuries, mostly governed by changes in land use, water management policies and hydroclimatic influence. The multi-proxy analysis of the paleolimnological record makes it possible to identify four main environmental stages

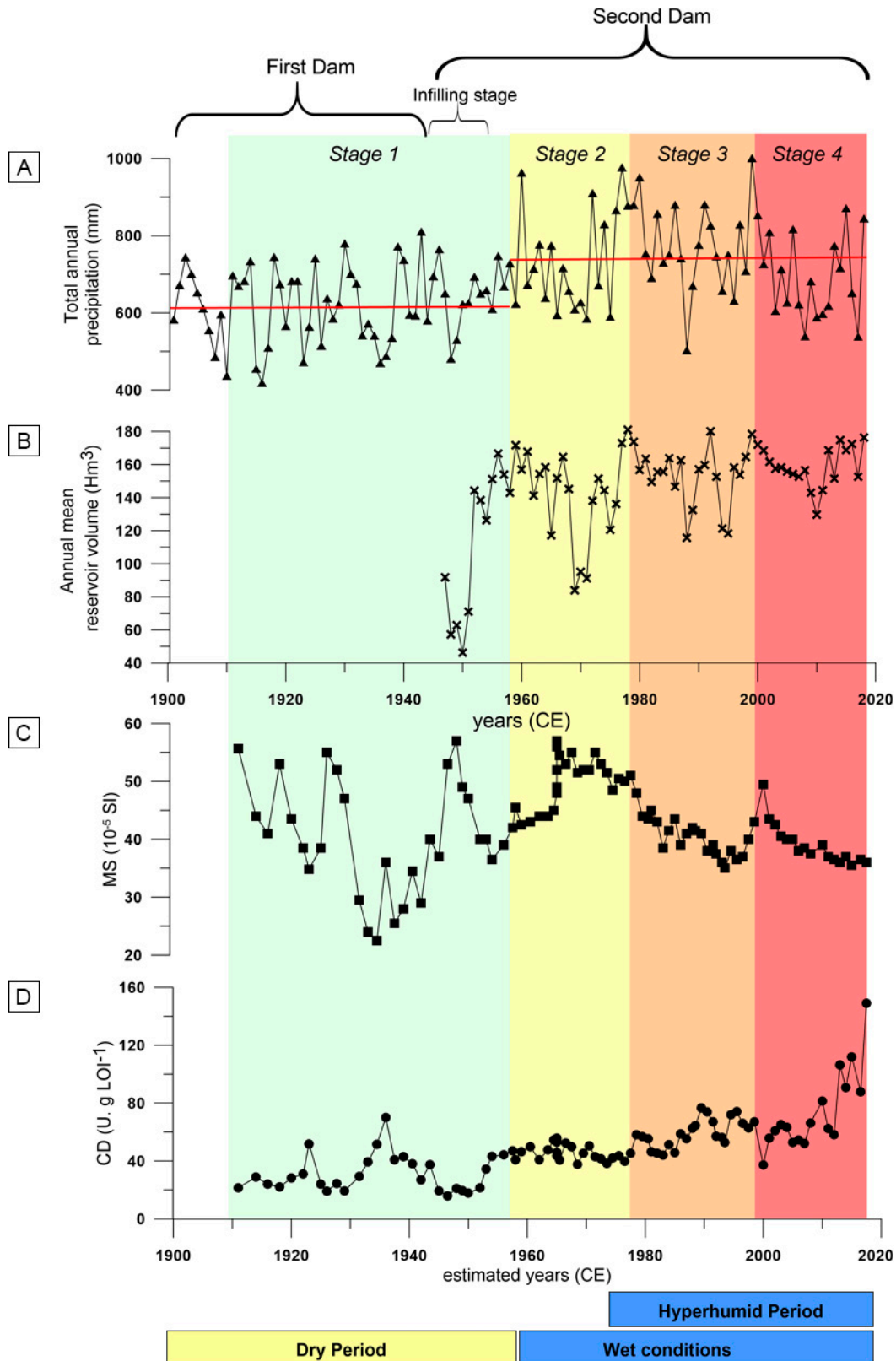


Figure 7. a) Total annual precipitation (millimeters, mm) of 31.25 S, 64.25 W region for 1901–2018 CE. Mean precipitation for 1901–1958 CE and 1959–2018 CE are indicated with red lines. b) Annual mean reservoir volume (cubic hectometers, Hm³) of San Roque reservoir for 1947–2018 CE. c) Magnetic susceptibility (MS, 10⁻⁵ SI units) determined on TSR-18-I. d) Chlorophyll derivatives (CD, U. g LOI⁻¹) determined on TSR-18-I. The color bands indicate the different stages: light green (Stage 1), yellow (Stage 2), orange (Stage 3), red (Stage 4). Above, first and second dam period and infilling stage are indicated. Below, the dry, wet and hyper humid period are shown.

throughout the history of the SRr. The two first stages (from 1911 to 1978 CE) were mainly controlled by natural drivers such as hydroclimatic conditions along with secondary anthropic influence, such as those related to changes in reservoir volume. The last two stages (1978–2018 CE) were mostly controlled by anthropic forcing, associated with the urban development in the catchment.

Stage 1 (1911–1958 CE), recorded by sedimentary facies D, can be considered the environmental base level of the reservoir since the anthropic impact was the lowest of all stages. During this stage, the input of organic matter derived mostly from littoral vegetation, and the low volume of the reservoir favored the accumulation of coarse-grain fluvial sediments. Stage 2 (1958–1978 CE), with dominant pelagic sedimentation, represents a change to a larger reservoir volume after the second dam was built. The low content of organic matter showed low primary production from allochthonous inputs. At the end of the stage, a generalized increase of regional precipitation took place. Stage 3 (1978–2000 CE), is characterized by an increase in the internal primary production, mainly caused by an anthropic input of nutrients due to urban expansion. Consequently, a higher level of eutrophication (eutrophic state) than the previous stages characterizes this period. Stage 4 (2000–2018 CE) corresponds to the highest trophic scenario in the SRr, which has led to a hypereutrophic state. This is mainly associated with the increase in urbanization throughout the catchment, especially in the littoral area of the reservoir.

The environmental reconstruction of the SRr makes it possible to identify multiple types of disturbances over time, including the enlargement of the reservoir's water volume and the increase of nutrient load due to increased urbanization. In addition, the great hydroclimatic jump after the 70s favored the maintenance of a lacustrine zone and the increase of nutrient input from the catchment. It is therefore likely that anthropic and natural forcing synergistically promoted the generalized degradation of the water quality in the SRr.

Future research should focus on a detailed analysis of the temporal changes in land use throughout the SRr catchment to infer their effects on its water quality and distinguish synergic couplings with natural forcing. Our results can provide tools not only to model future scenarios but also to establish watershed management policies. In

the future, climatic changes and population increase will play a determining role in access to drinking water. In South America, an effective land use policy in fluvial catchments should consider the climatic condition and assume measures aimed at mitigating eutrophication (i.e., controlling the nutrient sources by sewage treatments, the deforestation, the soil erosion and fires) along with the application of territorial ordering plans.

Acknowledgements

This research was conducted at CICTERRA (Consejo Nacional de Investigaciones Científicas y Técnicas – CONICET/Universidad Nacional de Córdoba – UNC) and CEPROCOR (Ministerio de Ciencia y Técnica – Gobierno de Córdoba). The study was supported by Agencia Nacional de Promoción Científica y Tecnológica (PICT-2013-1371 and PICT-2014-3298), CONICET (PUE-2016-CICTERRA), Secretaría de Ciencia y Técnica – UNC (PRIMAR-TP 2018-2020 and SECYTCONSOLIDAR- 2018- 411-18).

Support was provided to L.M. and I.C. by doctoral fellowships from CONICET (Argentina), of which this research is part. We would like to thank Dirección de Seguridad Náutica (Córdoba, Argentina) for supporting the fieldwork and Instituto Nacional del Agua – Centro de la Región Semiárida for providing hydrometeorological and water quality monitoring data. We acknowledge Nerina Pisani and Ivana Tapia for their help in the initial core description and to Mario Ravera (CEPROCOR) for facilitate us the SRr's bathymetry technical report, which was supported by Agencia Nacional de Promoción Científica y Tecnológica (FONARSEC: Fits 2013-0018). We also thank the comments and suggestions of the Editor and E. Chapron, which helped improve the manuscript.

REFERENCES

- Ballester, R. (1931). Proyecto del nuevo dique San Roque. *Revista de la Universidad Nacional de Córdoba* 18 (1-2): 42–65. [Project of the new San Roque Dam].
- Binford, M. W., Kahl, J. S. and Norton, S. A. (1993). Interpretation of ²¹⁰Pb profiles and verification of the CRS dating model in PIRLA project lake sediment cores. *Journal of Paleolimnology*, 9 (3): 275-296.
- Birks, H.H. and Birks, H.J.B. (2006). Multi-proxy studies in palaeolimnology. *Vegetation History and Archaeobotany* 15 (4): 235–251.
- Bonanssea, M. and Fernandez, R.L. (2013). Remote sensing of

- suspended solids concentration in a reservoir with frequent wildland fires on its watershed. *Water Science and Technology* 67 (1): 217–223.
- Bonetto, A.A., Di Persia, D.H., Maglianesi, R. and Corigliano, M. del C. (1976). Caracteres limnológicos de algunos lagos eutróficos de embalse de la Región Central de Argentina. *ECOSUR* 3(5): 83–98. [Limnological characters of some eutrophic reservoirs in the Central Region of Argentina].
- Brahney, J., Clague, J.J., Menounos, B. and Edwards, T.W.D. (2008). Timing and cause of water level fluctuations in Kluane Lake, Yukon Territory, over the past 5000 years. *Quaternary Research* 70 (2): 213–227.
- Cabido, M. and Zak, M.R. (1999). Vegetación del norte de Córdoba. SAGyRR. 52 pp. [Vegetation of Córdoba north].
- Cabrera, A.L. (1971). Fitogeografía de la República Argentina. *Boletín de la Sociedad Argentina de Botánica* 14 (1-2): 1–42. [Phytogeography of Argentinian republic].
- Cachi, J.C. (1975). Variaciones plantónicas del Embalse San Roque (Córdoba- República Argentina) y su relación con los procesos de potabilización. [Planktonic variations of San Roque reservoir (Córdoba-Argentina) and its relationship with purification process].
- Camilloni, I.A. and Barros, V.R. (2003). Extreme discharge events in the Paraná River and their climate forcing. *Journal of Hydrology* 278 (1-4): 94–106.
- Cardoso-Silva, S., López-Doval, J.C., Moschini-Carlos, V. and Pompêo, M. (2018). Metals and limnological variables in an urban reservoir: compartmentalization and identification of potential impacted areas. *Environmental Monitoring and Assessment* 190 (1): 1–13.
- Carpenter, S.R. and Leavitt, P.R. (1991). Temporal variation in a paleolimnological record arising from a trophic cascade. *Ecology* 72 (1): 277–285.
- Cohen, A. (2003). *Paleolimnology: The History and Evolution of Lake Systems*. Oxford University Press, 528 pp.
- Colladón, L. (2004). Estadística Meteorológica, Temperaturas Medias Mensuales 1994-2003, Cuenca del Río San Antonio. Villa Carlos Paz. [Meteorological Statistics, Monthly Average Temperatures 1994-2003, Basin of San Antonio river].
- Colladón, L. (2014). Síntesis Pluviométrica 1992-2012, Cuenca del Río San Antonio: Sistema del Río Suquia, Provincia de Córdoba. [Pluviometric Synthesis 1992-2012, Basin of San Antonio river: Suquia River system, Province of Córdoba].
- Compagnucci, R.H., Agosta, E.A. and Vargas, W.M. (2002). Climatic change and quasi-oscillations in central-west Argentina summer precipitation: Main features and coherent behaviour with southern African region. *Climate Dynamics* 18 (5): 421–435.
- Costa-Böddeker, S., Bennion, H., Araújo de Jesus, T., Albuquerque, A.L.S., Figueira, R.C.L. and Bicudo, D. de C. (2012). Paleolimnologically inferred eutrophication of a shallow, tropical, urban reservoir in southeast Brazil. *Journal of Paleolimnology* 48 (4): 751–766.
- Dasso, C.M., Piovano, E.L., Pasquini, A.I. and Córdoba, F.E. (2014). Recursos hídricos superficiales. *Relatorio del XIX Congreso Geológico Argentino* 1209–1231. [Surface water resources].
- Dean, W.E. (1974). Determination of carbonate and organic matter in calcareous sediments and sedimentary rocks by loss of ignition: comparison with other methods. *Journal of Sedimentary Petrology* 44 (1): 242–248.
- Dearing, J.A. (2013). Why Future Earth needs lake sediment studies. *Journal of Paleolimnology* 49 (3): 537–545.
- Deon, J.U. (2015). Sierras Chicas, conflictos por el agua y el uso del suelo. Relaciones de poder en la gestión de cuencas. El caso de la cuenca del río Chavascate, Córdoba, Argentina. *Revista del Departamento de Geografía* 4 (1): 162–189. [Conflicts for water and land use. Power relations in watershed management. The case of the river basin Chavascate, Córdoba, Argentina].
- Dokulil, M.T. (1994). Environmental control of phytoplankton productivity in turbulent turbid systems. In: Descy, J.-P., C.S. Reynolds and J. Padisák (Eds.), *Phytoplankton in Turbid Environments: Rivers and Shallow Lakes*, Springer Dordrecht, pp. 65–72.
- Dubois, N., Saulnier-Talbot, É., Mills, K., Gell, P., Battarbee, R., Bennion, H., Chawchai, S., Dong, X., Francus, P., Flower, R., Gomes, D.F., Gregory-Eaves, I., Humane, S., Kattel, G., Jenny, J.P., Langdon, P., Massaferró, J., McGowan, S., Mikomägi, A., Ngoc, N.T.M., Ratnayake, A.S., Reid, M., Rose, N., Saros, J., Schillereff, D., Tolotti, M. and Valero-Garcés, B. (2018). First human impacts and responses of aquatic systems: A review of palaeolimnological records from around the world. *Anthropocene Review* 5 (1): 28–68.
- Egeland, E.S., Garrido, J.L., Clementson, L., Andresen, K., Thomas, C.S., Zapata, M., Airs, R., Llewellyn, C.A., Newman, G.L., Rodríguez, F. and Roy, S. (2011). Data sheets aiding identification of phytoplankton carotenoids and chlorophylls in collaboration with. In: Roy, S., C. Llewellyn, E. Egeland and G. Johnsen (Eds.), *Phytoplankton pigments: Characterization, Chemotaxonomy and Applications in Oceanography*, Cambridge University Press, Cambridge, UK, pp. 665–822.
- Elchyshyn, L., Goyette, J.O., Saulnier-Talbot, É., Maranger, R., Nozais, C., Solomon, C.T. and Gregory-Eaves, I. (2018). Quantifying the effects of hydrological changes on long-term water quality trends in temperate reservoirs: insights from a multiscale, paleolimnological study. *Journal of Paleolimnology* 60 (3): 361–379.
- Foucher, A., Evrard, O., Cerdan, O., Chabert, C., Lecompte, F., Lefèvre, I., Vandromme, R. and Salvador-Blanes, S. (2020). A quick and low-cost technique to identify layers associated with heavy rainfall in sediment archives during the Anthropocene. *Sedimentology*, 67(1), 486–501.
- Gangi, D., Plastani, M.S., Laprida, C., Lami, A., Dubois, N., Bordet, F., Gogorza, C., Frau, D. and de Tezanos Pinto, P. (2020). Recent cyanobacteria abundance in a large sub-tropical reservoir inferred from analysis of sediment cores. *Journal of Paleolimnology* 63 (3): 195–209.
- García de Emiliani, M.O. (1977). Ciclo anual del fitoplancton en el Embalse San Roque (Córdoba, Argentina). *Revista Asociación Ciencias Naturales Litoral* 8: 1–12. [Annual cycle of phytoplankton in the San Roque Reservoir (Córdoba, Argentina)].
- Garreaud, R.D. (2009). The Andes climate and weather. *Advances in Geosciences* 22: 3–11.
- Gavilán, J.G. (1981). Study water quality in the San Roque reservoir. *Water Qual. Bull. Environ.* 6 (4), 136–158.
- Gómez, E.A., Raniolo, L.A., Pierini, J.O., Pons, J.C. (2016). Batimetría y perfilado sísmico en el Lago San Roque-Córdoba. Informe técnico Instituto Argentino de Oceanografía-Conicet. [Bathymetry and seismic profiling in San Roque Lake-Córdoba].
- Guerra, L., Piovano, E.L., Córdoba, F.E., Sylvestre, F. and Damatto Moreira, S. (2015). The hydrological and environmental evolution of shallow Lake Melincué, central Argentinean Pampas, during the last millennium. *Journal of Hydrology* 529:

- 570–583.
- Guerra, L., Piovano, E.L., Córdoba, F.E., Tachikawa, K., Rostek, F., Garcia, M., Bard, E. and Sylvestre, F. (2016). Climate change evidences from the end of the Little Ice Age to the Current Warm Period registered by Melincué Lake (Northern Pampas, Argentina). *Quaternary International* 438: 160–174.
- Guerra, L., Martini, M.A., Córdoba, F.E., Ariztegui, D. and Piovano, E.L. (2018). Multi-annual response of a Pampean shallow lake from central Argentina to regional and large-scale climate forcings. *Climate Dynamics* 52 (11): 6847–6861.
- Guilizzoni, P., Bonomi, G., Galanti, G. and Ruggiu, D. (1983). Relationship between sedimentary pigments and primary production: evidence from core analyses of twelve Italian lakes. *Hydrobiologia* 103: 103–106.
- Guilizzoni, P. and Lami, A. (2003). Paleolimnology: use of algal pigments as indicators. In: Bitton, G. (Ed.), *Encyclopedia of Environmental Microbiology*, Wiley and Sons, Chichester, pp. 2306–2317.
- Halac, S., Bazán, R., Larrosa, N., Nadal, A.F., Ruibal Conti, A.L., Rodriguez, M.I., Ruiz, M. and Lopéz, A.G. (2019). First report on negative association between cyanobacteria and fecal indicator bacteria at San Roque reservoir (Argentina): impact of environmental factors. *Journal of Freshwater Ecology* 34 (1): 273–291.
- Halac, S., Mengo, L., Guerra, L., Lami, A., Musazzi, S., Loizeau, J.L., Ariztegui, D. and Piovano, E.L. (2020). Paleolimnological reconstruction of the centennial eutrophication processes in a sub-tropical South American reservoir. *Journal of South American Earth Sciences* 103: 102707.
- Harris, I., Osborn, T.J., Jones, P. and Lister, D. (2020). Version 4 of the CRU TS monthly high-resolution gridded multivariate climate dataset. *Scientific Data* 7 (1): 1–18.
- Heiri, O., Lotter, A.F. and Lemcke, G. (2001). Loss on ignition as a method for estimating organic and carbonate content in sediments: reproducibility and comparability of results. *Journal of Paleolimnology* 25 (1): 101–110.
- Hodgson, D.A., Vyverman, W. V., Verleyen, E., Sabbe, K., Leavitt, P.R., Taton, A., Squier, A.H. and Keely, B.J. (2004). Environmental factors influencing the pigment composition of in situ benthic microbial communities in east Antarctic lakes. *Aquatic Microbial Ecology* 37(3): 247–263.7
- Jongman, R. H. J., ter Braak, C.J.F., and Van Tongeren, O. F. R. (1995). *Data Analysis in Community and Landscape Ecology*. Cambridge University Press. 299 pp.
- Juggins, S. (2009). Rioja: analysis of quaternary science data, R package version 0.5–6.
- Kennedy, R.H. (2005). Toward integration in reservoir management. *Lake and Reservoir Management* 21 (2): 128–138.
- Krasa, J., Dostal, T., Jachymova, B., Bauer, M. and Devaty, J. (2019). Soil erosion as a source of sediment and phosphorus in rivers and reservoirs – Watershed analyses using WaTEM/SEDEM. *Environmental Research* 171: 470–483.
- Lami, A., Guilizzoni, P. and Marchetto, A. (2000). High resolution analysis of fossil pigments, carbon, nitrogen and sulphur in the sediment of eight European Alpine lakes: The MOLAR project. *Journal of Limnology* 59 (1): 15–28.
- Lami, A., Niessen, F., Guilizzoni, P., Masafarro, J. and Belis, C.A. (1994). Palaeolimnological studies of the eutrophication of volcanic Lake Albano (Central Italy). *Journal of Paleolimnology* 10 (3): 181–197.
- Leavitt, P.R. (1993). A review of factors that regulate carotenoid and chlorophyll deposition and fossil pigment abundance. *Journal of Paleolimnology* 9 (2): 109–127.
- Liu, X., Wu, Q., Chen, Y. and Dokulil, M.T. (2011). Imbalance of plankton community metabolism in eutrophic Lake Taihu, China. *Journal of Great Lakes Research* 37 (4): 650–655.
- Martino, R.D., Guereschi, A.B. and Carignano, C.C. (2012). Influencia de la tectónica preandina sobre la tectónica Andina: El caso de la falla de la Sierra Chica, Sierras Pampeanas de Córdoba. *Revista de la Asociación Geológica Argentina* 69 (2): 207–221.
- Menounos, B. (1997). The water content of lake sediments and its relationship to other physical parameters: an alpine case study. *The Holocene* 7 (2): 207–212.
- Merlo, C., Abril, A., Amé, M. V., Argüello, G.A., Carreras, H.A., Chiappero, M.S., Hued, A.C., Wannaz, E., Galanti, L.N., Monferrán, M. V., González, C.M. and Solís, V.M. (2011). Integral assessment of pollution in the Suquia River (Córdoba, Argentina) as a contribution to lotic ecosystem restoration programs. *Science of the Total Environment* 409 (23): 5034–5045.
- Monferrán, M.V., Galanti, L.N., Bonansea, R.I., Amé, M.V. and Wunderlin, D.A. (2011). Integrated survey of water pollution in the Suquia River basin (Córdoba, Argentina). *Journal of Environmental Monitoring* 13 (2): 398–409.
- Moorhouse, H.L., McGowan, S., Taranu, Z.E., Gregory-Eaves, I., Leavitt, P.R., Jones, M.D., Barker, P. and Brayshaw, S.A. (2018). Regional versus local drivers of water quality in the Windermere catchment, Lake District, United Kingdom: The dominant influence of wastewater pollution over the past 200 years. *Global Change Biology* 24 (9): 4009–4022.
- Obst, M., Wehrli, B. and Dittrich, M. (2009). CaCO₃ nucleation by cyanobacteria: Laboratory evidence for a passive, surface-induced mechanism. *Geobiology* 7 (3): 324–347.
- Oksanen, J., F. Guillaume Blanchet, R.K., Legendre, P., Minchin, P.R., O'Hara, R.B., Simpson, G.L., Solymos, P. and M. Henry H. Stevens, H.W. (2019). Package 'vegan'. *R Package Version 3.4.0*.
- Oliver, S., Corburn, J. and Ribeiro, H. (2019). Challenges regarding water quality of eutrophic reservoirs in urban landscapes: A mapping literature review. *International Journal of Environmental Research and Public Health* 16 (1):40.
- Padedda, B.M., Sechi, N., Lai, G.G., Mariani, M.A., Pulina, S., Sarria, M., Satta, C.T., Viridis, T., Buscarinu, P. and Lugliè, A. (2017). Consequences of eutrophication in the management of water resources in Mediterranean reservoirs: A case study of Lake Cedrino (Sardinia, Italy). *Global Ecology and Conservation* 12: 21–35.
- Pasquini, A.I., Lecomte, K.L., Piovano, E.L. and Depetris, P.J. (2006). Recent rainfall and runoff variability in central Argentina. *Quaternary International* 158 (1): 127–139.
- Paterson, A.M., Köster, D., Reavie, E.D. and Whitmore, T.J. (2020). Preface: paleolimnology and lake management. *Lake and Reservoir Management* 36 (3): 205–209.
- Pienitz, R. and Vincent, W.F. (2003). Generic approaches towards water quality monitoring based on paleolimnology. In: Kumagai, M. and W.F. Vincent (Eds.), *Freshwater management: global versus local perspectives*, Springer-Verlag, Tokyo, pp. 61–82.
- Pienitz, R. and Lotter, A.F. (2009). Editorial: Advances in Paleolimnology. *PAGES News* 17 (3): 92–93.
- Piovano, E.L., Larizzatti, F.E., Fávoro, D.I.T., Oliveira, S.M.B., Damatto, S.R., Mazzilli, B.P. and Ariztegui, D. (2004). Geochemical response of a closed-lake basin to 20 th century recurring droughts / wet intervals in the subtropical Pampean Plains of South America. *Journal of Limnology* 63 (1): 21–32.

- Piovano, E.L., Ariztegui, D., Córdoba, F.E., Cioccale, M. and Sylvestre, F. (2009). Hydrological variability in South America below the Tropic of Capricorn (Pampas and eastern Patagonian, Argentina) during the last 13.0 ka. In: Vimeux, F., F. Sylvestre and M. Khodri (Eds.), *Past climate variability from the Last Glacial Maximum to the Holocene in South America and Surrounding regions: From the Last Glacial Maximum to the Holocene*, Springer Developments in Paleoenvironmental Research Series, pp. 323–351.
- Prosperi, C. (1986). Algas en el agua de consumo de la Ciudad de Córdoba. *Boletín de la Sociedad Argentina de Botánica* 24 (3-4): 413–417.
- Pussetto, N., Piovano, E.L., Rodríguez, M.I., Ruiz, M. and Halac, S. R. (2020). Modelo conceptual del funcionamiento del embalse San Roque: dinámica sedimentaria y geoquímica. *Revista de la Facultad de Ciencias Exactas Físicas y Naturales* 7 (2): 85–94.
- Renaut, R.W. and Gierlowski-Kodersch, E.H. (2010). Lakes. In: James, N.P. and R.W.
- Dalrymple (Eds.), *Facies Models 4*, Canadian Sedimentology Research Group, pp. 541–575.
- Rodríguez, M.I. and Ruiz, M. (2016). Limnology of the San Roque Reservoir. In: Wunderlin, D. (Ed.), *The Suquia River Basin (Córdoba, Argentina). The Handbook of Environmental Chemistry*, Springer, Cham, pp. 37–59.
- Roldán Pérez, G. and Ramírez Restrepo, J.J. (2008). *Fundamentos de Limnología Neotropical*. Universidad de Antioquía. 440 pp. [Neotropical Limnology Basics].
- Saulnier-Talbot, É. (2016). Paleolimnology as a tool to achieve environmental sustainability in the Anthropocene: an overview. *Geosciences* 6 (2): 26.
- Schnurrenberger, D., Russell, J. and Kelts, K. (2003). Classification of lacustrine sediments based on sedimentary components. *Journal of Paleolimnology* 29 (2): 141–154.
- Schroeder, L.A., Martin, S.C., Kerns, G.J. and McLean, C.E. (2016). Diatom assemblages in a reservoir sediment core track land-use changes in the watershed. *Journal of Paleolimnology* 55 (1): 17–33.
- Smol, J.P. (2010). The power of the past: Using sediments to track the effects of multiple stressors on lake ecosystems. *Freshwater Biology* 55 (1): 43–59.
- Teranes, J.L., McKenzie, J.A., Lotter, A.F. and Sturm, M. (1999). Stable isotope response to lake eutrophication: Calibration of a high-resolution lacustrine sequence from Baldeggersee, Switzerland. *Limnology and Oceanography* 44 (2): 320–333.
- Thompson, J.B., Schultze-Lam, S., Beveridge, T.J. and Des Marais, D.J. (1997). Whiting events: Biogenic origin due to the photosynthetic activity of cyanobacterial picoplankton. *Limnology and Oceanography* 42(1): 133–141.
- Tripaldi, A., Zárate, M.A., Forman, S.L., Badger, T., Doyle, M.E. and Ciccioli, P. (2013). Geological evidence for a drought episode in the western Pampas (Argentina, South America) during the early-mid 20th century. *The Holocene* 23 (12): 1731–1746.
- Troin, M., Vallet-Coulomb, C., Sylvestre, F. and Piovano, E. (2010). Hydrological modelling of a closed lake (Laguna Mar Chiquita, Argentina) in the context of 20th century climatic changes. *Journal of Hydrology* 393 (3-4): 233–244.
- Troin, M., Vrac, M., Khodri, M., Caya, D., Vallet-Coulomb, C., Piovano, E.L. and Sylvestre, F. (2016). A complete hydroclimate model chain to investigate the influence of sea surface temperature on recent hydroclimatic variability in subtropical South America (Laguna Mar Chiquita, Argentina). *Climate Dynamics* 46 (5-6): 1783–1798.
- Turgeon, K., Solomon, C.T., Nozais, C. and Gregory-Eaves, I. (2016). Do novel ecosystems follow predictable trajectories? Testing the trophic surge hypothesis in reservoirs using fish. *Ecosphere* 7 (12): 1–17.
- Wang, L.C., Chou, Y.M., Chen, H.F., Chang, Y.P., Chiang, H.W., Yang, T.N., Shiau, L.J. and Chen, Y.G. (2021). Paleolimnological evidence for lacustrine environmental evolution and paleo-typhoon records during the late Holocene in eastern Taiwan. *Journal of Paleolimnology* 1–17.
- Wengrat, S., Padiál, A.A., Jeppesen, E., Davidson, T.A., Fontana, L., Costa-Bóddeker, S. and Bicudo, D.C. (2018). Paleolimnological records reveal biotic homogenization driven by eutrophication in tropical reservoirs. *Journal of Paleolimnology* 60 (2): 299–309.
- Wengrat, S., Bennion, H., Ferreira, P.A. de L., Figueira, R.C.L. and Bicudo, D.C. (2019). Assessing the degree of ecological change and baselines for reservoirs: challenges and implications for management. *Journal of Paleolimnology* 62 (4): 337–357.
- Winston, B., Hausmann, S., Escobar, J. and Kenney, W.F. (2014). A sediment record of trophic state change in an Arkansas (USA) reservoir. *Journal of Paleolimnology* 51 (3): 393–403.
- Woodbridge, J., Davies, H.J., Blake, W.H. and Fyfe, R.M. (2014). Recent environmental change in an upland reservoir catchment: a palaeoecological perspective. *Journal of Paleolimnology* 52 (3): 229–244.
- Xu, Z., Cai, X., Yin, X., Su, M., Wu, Y. and Yang, Z. (2019). Is water shortage risk decreased at the expense of deteriorating water quality in a large water supply reservoir? *Water Research* 165: 114984.
- Ye, Y., He, X.Y., Chen, W., Yao, J., Yu, S. and Jia, L. (2014). Seasonal water quality upstream of Dahuofang Reservoir, China - the effects of land use type at various spatial scales. *CLEAN- Soil, Air, Water* 42 (10): 1423–1432.
- Züllig, H. (1985). Carotenoids from plankton and purple sulphur bacteria in lake sediments as indicators of changes in the environment. *Experientia* 41 (4): 533–534.